Supporting Information

Monolithically Integrated Perovskite Semiconductor Lasers on Silicon Photonic Chips by Scalable Top-Down Fabrication

†Piotr J. Cegielski, †Anna Lena Giesecke, ‡Stefanie Neutzner, †Caroline Porschatis, ‡Marina Gandini, †Daniel Schall, ‡Carlo A. R. Perini, †Jens Bolten, †Stephan Suckow, §Satender Kataria, †Bartos Chmielak, †Thorsten Wahlbrink, ‡Annamaria Petrozza, §Max C. Lemme*

†AMO GmbH, Otto-Blumenthal-Straße 25, 52074 Aachen, Germany, *E-mail: giesecke@amo.de

‡Center for Nano Science and Technology @Polimi, Istituto Italiano di Tecnologia, via Giovanni Pascoli 70/3, 20133 Milan, Italy

§RWTH Aachen University, Elektrotechnik und Informationstechnik, Lehrstuhl für Elektronische Bauelemente, Otto-Blumenthal-Str. 25, 52074 Aachen, Germany

Table of Contents

I.	**Analytical calculations of whispering gallery modes**	**2**
II.	**Refractive index measurements**	**4**
III.	**Design by numerical simulations**	**6**
IV.	**Laser characterization - figures**	**10**
V.	**References:**	**13**

I. Analytical calculations of whispering gallery modes

Spectral positions of whispering gallery modes (WGM, Figure S 1) were found analytically by solving 2D Maxwell equations in a cylindrical coordinate system[1] using effective refractive index (n_{eff}) method[2], in which refractive index of 3D perovskite disc was approximated by n_{eff} of slab waveguide mode for TM and TE polarizations respectively. Disc resonators support transverse electric (TE) and transverse magnetic (TM) mode families listed in Table S 1 and S 2.

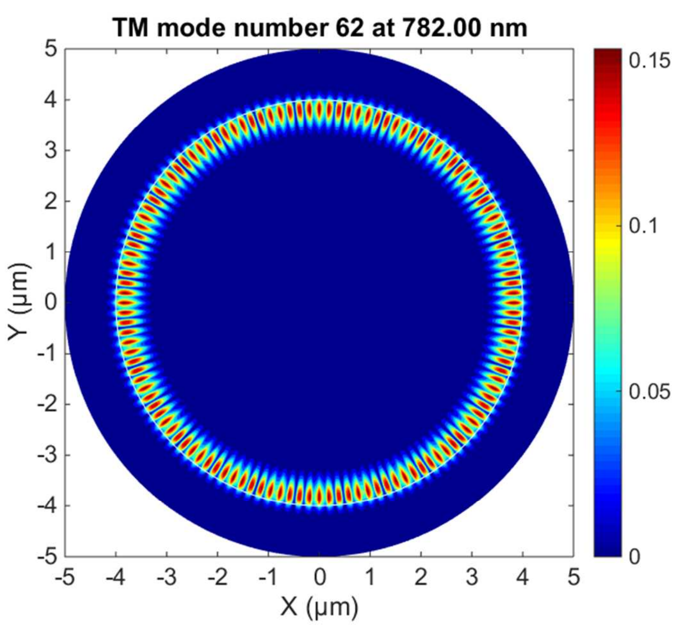

Figure S 1 Amplitude of the electric field of 62nd TM mode of a perovskite disc resonator with radius = 4 µm. The disc is outlined with the white line.

Table S 1 Calculated TE modes of perovskite disc resonators.

Disc radius (μm)	Longitudinal TE mode number	Resonant wavelength	n_{eff}	FSR
4	63	801.73	2.14	7.90
	64	794.43	2.16	7.30
	65	787.87	2.16	6.56
	66	782.48	2.18	5.39
	67	777.72	2.20	4.77
	68	772.43	2.22	5.29
6	98	800.27	2.16	5.05
	99	795.48	2.18	4.79
	100	790.00	2.18	4.48
	101	786.89	2.18	4.10
	102	783.37	2.20	3.52
	103	780.22	2.22	3.15
	104	777.08	2.22	3.14
	105	773.66	2.23	3.41
8	130	800.44	2.15	3.74
	131	796.84	2.16	3.60
	132	793.40	2.17	3.44
	133	790.15	2.19	3.25
	134	787.12	2.20	3.03
	135	784.41	2.20	2.70
	136	782.00	2.21	2.42
	137	779.68	2.23	2.31
	138	777.34	2.25	2.33
	139	774.87	2.24	2.47
	140	772.10	2.24	2.78

Table S 2 Calculated TM modes of perovskite disc resonators.

Disc radius (μm)	Longitudinal TM mode number	Resonant wavelength	n_{eff}	FSR
4	59	800.5786	1.99	7.61
	60	793.5269	2.00	7.05
	61	787.20	2.01	6.33
	62	782.00	2.03	5.20
	63	777.28	2.06	4.71
	64	772.00	2.08	5.28
6	91	797.62	2.02	4.79
	92	793.08	2.02	4.54
	93	788.86	2.03	4.22
	94	785.08	2.05	3.78
	95	781.83	2.06	3.26
	96	778.74	2.07	3.09
	97	775.55	2.09	3.19
8	122	800.53	2.02	3.66
	123	797.01	2.03	3.52
	124	793.64	2.04	3.38
	125	790.42	2.04	3.21
	126	787.42	2.05	3.01
	127	784.70	2.06	2.71
	128	782.28	2.07	2.42
	129	779.98	2.07	2.30
	130	777.67	2.09	2.31
	131	775.26	2.10	2.41
	132	772.61	2.11	2.65

II. Refractive index measurements

MAPbI3 disc lasers were designed using refractive index values (Figure S 3) obtained by spectroscopic ellipsometry at 75.48° angle (J.A. Wollam M-2000 ellipsometer). The MAPbI3 was deposited on 1 mm soda lime substrates (Menzel-Gläser). Perovskite thickness was measured by scanning electron microscope (SEM) inspection of the sample cross-section. Fitting was performed using CompleteEase software with a 4 oscillator model. Back reflections were corrected by fitting depolarization. A mean squared error (MSE) of 3.1 was obtained for the best fit. Exact parameters are listed in Table S 3. Model included RMS surface roughness fit, which was found to be 8.28 nm.

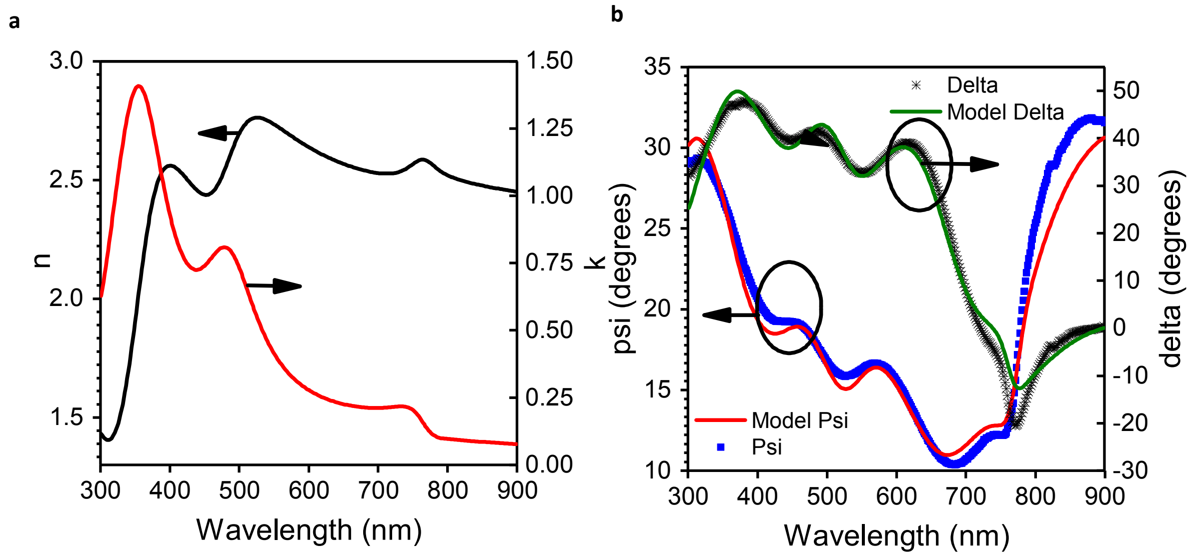

Figure S 2 a) Complex refractive index of $MAPbI_3$. b) Fit used to extract complex refractive index of $MAPbI_3$ from the ellipsometric measurement.

Table S 3 Parameters used to model the dielectric function of $MAPbI_3$

Oscillator	Parameter	Value (eV)
Tauc-Lorentz	Eg	1.56
	E_0	1.62
	A_0	22.78
	Γ_0	0.12
Lorentz	E_0	2.52
	A_0	2.75
	Γ_0	0.52
Lorentz	E_0	3.37
	A_0	5.72
	Γ_0	0.87
Harmonic	E_0	7.5
	A_0	20.96
	Γ_0	0.8

III. Design by numerical simulations

Bus waveguide modes were obtained by finite difference (FD) mode solver (Figure S 3a-b). The whispering gallery disc mode profiles (Figure S 3c-d) were obtained by calculating modes of a bent waveguide with the same radius as the disc and selecting a mode matching n_{eff} obtained by analytical calculation (Table S 1 and S 2).

Vertical directional couplers (see Figure 1 of the main text) were designed with help of finite difference time domain (FDTD) simulations via the commercial software package Lumerical. The simple model (Figure S 4a-b) consisted of a perovskite disc, a mode launcher which injected whispering gallery modes (Figure S 3c-d) and a silicon nitride bus waveguide with a mode monitor at the output. The mode expansion method (used as implemented in Lumerical) was used to extract coupling efficiencies between disc and waveguide modes of different polarizations.

Simulations were performed with varying position of the center of the bus waveguide with respect to the disc edge (called "offset") and height of the coupling gap (Figure S 4b). Coupling efficiency depends on the alignment of the bus waveguide with spatial location of the electric field maximum of the WGM. The maxima are located further from the disc edge, therefore coupling efficiency is the highest at offsets of -450 nm and -250 nm (negative offset means the waveguide is closer to the disc center) for TE and TM modes, respectively (Figure S 4c). Modes of the opposite polarizations than the WGMs are also excited, but they are 24 times or 6 times weaker than waveguide modes of the same polarizations as WGMs for TE and TM WGMs respectively. Coupling efficiency exponentially drops when the coupling gap increases reaching the plateau of low values at gaps larger than 100 nm (Figure S 4d), therefore it has to be kept low in the actual devices. It was decided to aim at 50 nm as a good compromise between reasonable coupling efficiency and risk of damaging the waveguides during the SiO_2 thinning by reactive ion etching process. The electric field amplitudes in the bus waveguide plane of TM and TE WGMs in the directional coupler are shown in Figure S 5. It can be seen that both TE and TM polarized WGMs couple well into the aligned waveguides (Figure S 5a and 5d) while misalignment leads to excitation of higher order modes which are radiating out of the structure (Figure S 5b) or to no coupling at all (Figure S 5c). In all cases some energy is reflected into the opposite direction in the bus waveguide. We found that the optimum offset is -150 nm, which allows reasonable coupling for both polarizations of WGMs.

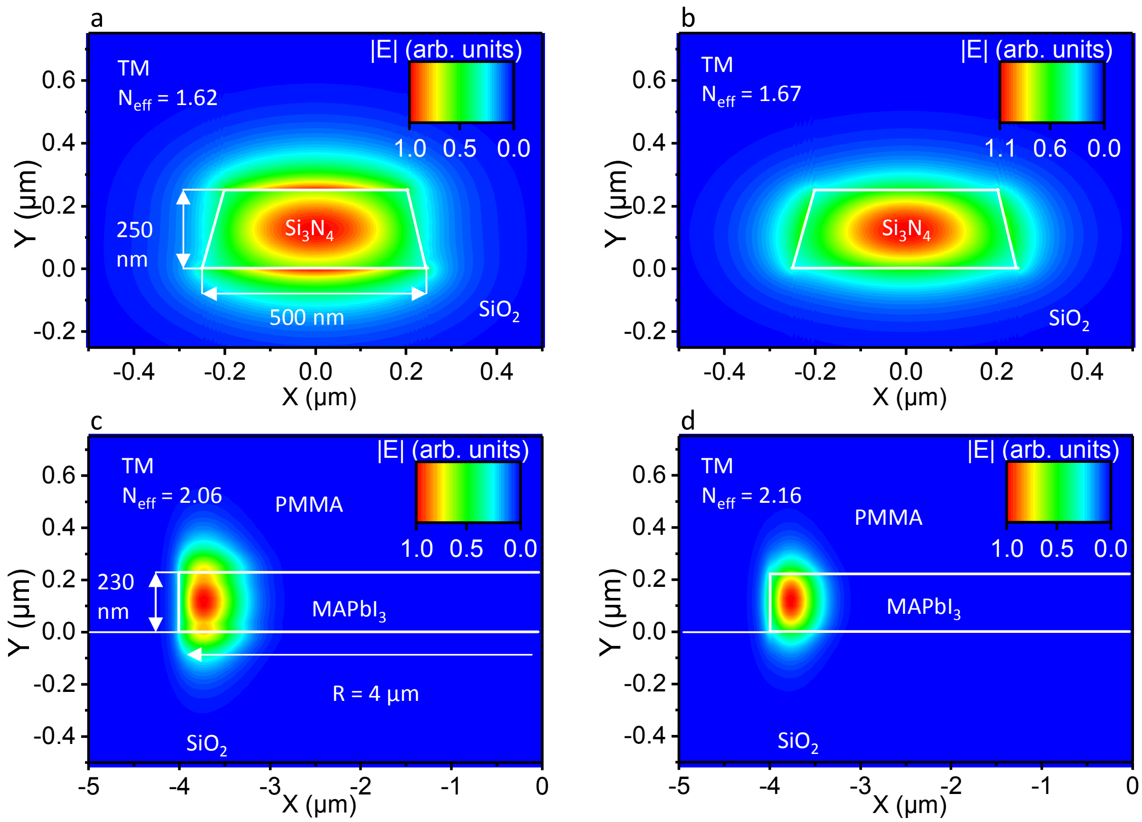

Figure S 3 Electric field amplitude distribution of: a) TM bus waveguide fundamental mode. b) TE bus waveguide fundamental mode. c) TM whispering gallery disc mode. d) TE whispering gallery disc mode.

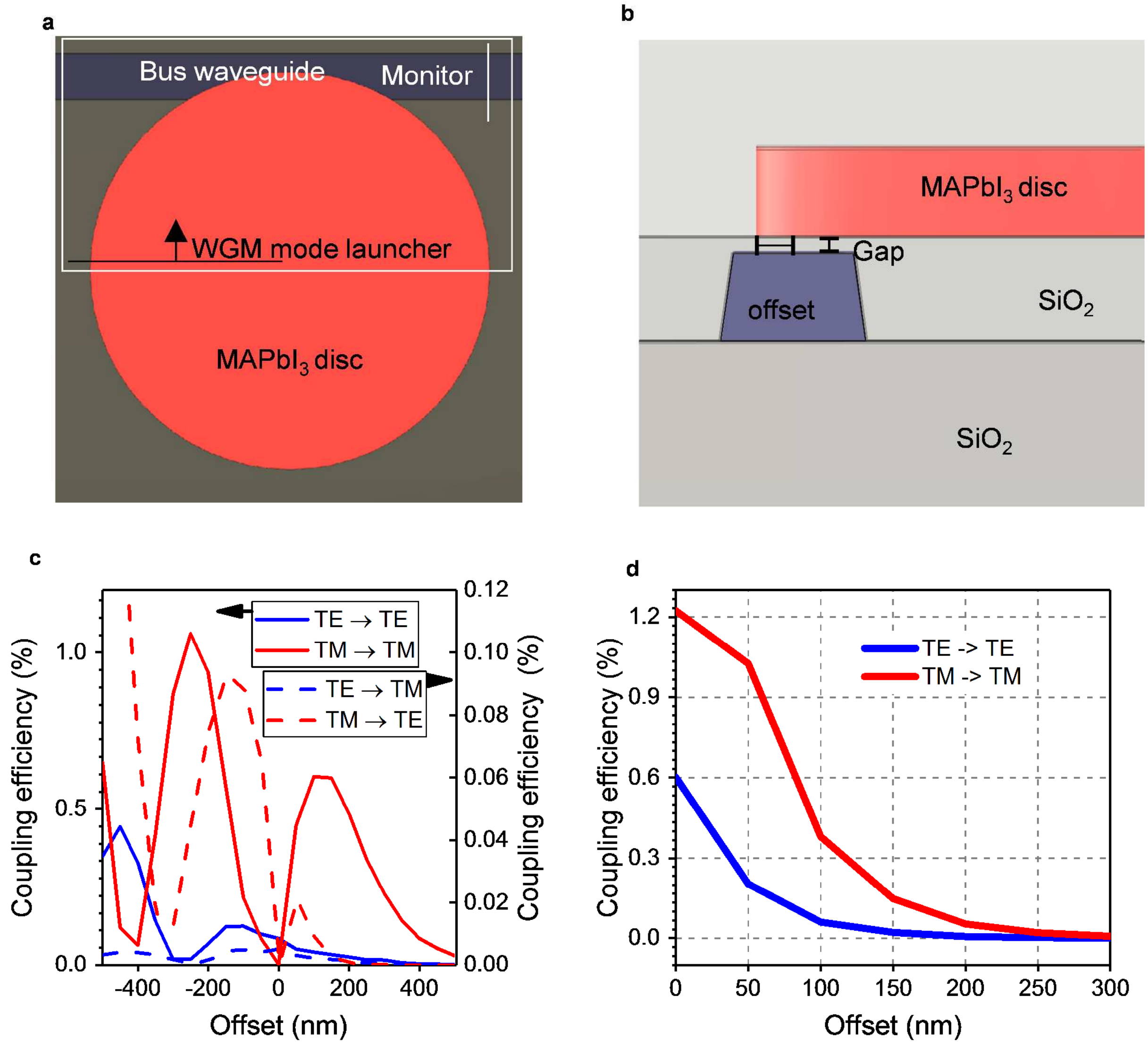

Figure S 4 a) Schematic of simulation model of the vertical directional coupler. b) cross-section of the simulation model. c) Coupling efficiency of disk modes to WGMs of corresponding polarization (left axis, solid lines) and to the opposite polarization (right axis, dashed lines), dependent on the offset of bus waveguide position. Negative offset means that the waveguide is closer to the disc center d) Coupling efficiency dependency on the height of the vertical coupling gap.

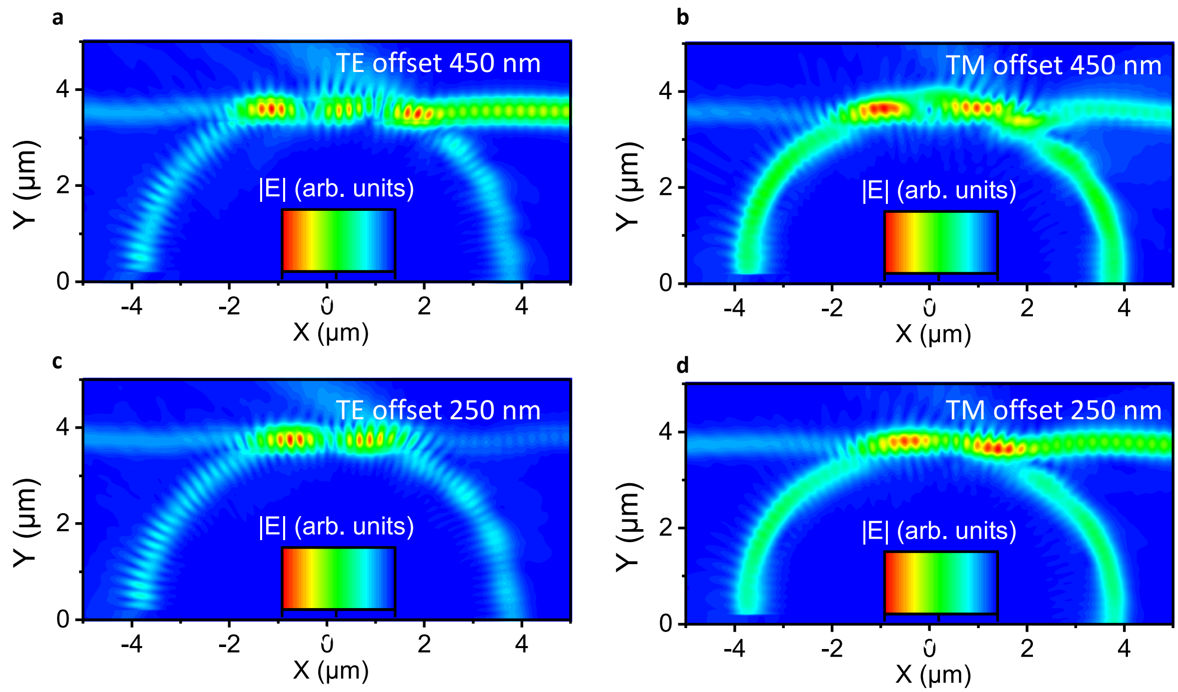

Figure S 5 Electric field amplitude in the bus waveguide plane of the directional coupler: a) TE WGM, offset = 450 nm. b) TM WGM offset 450 nm. c) TE WGM offset 250 nm, d) TM WGM offset 250 nm.

IV. Laser characterization - figures

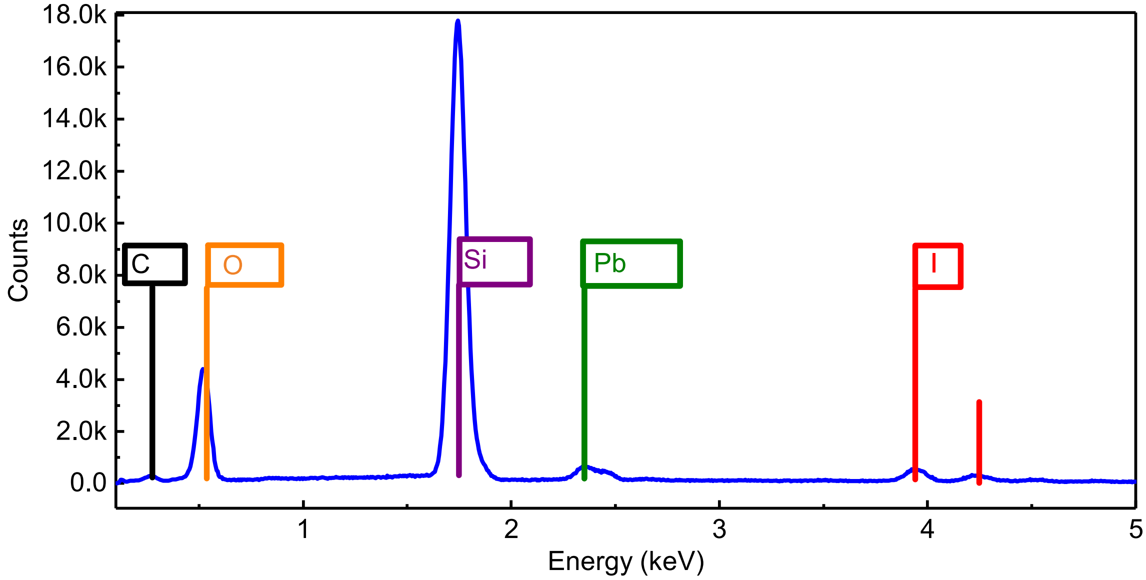

Figure S 6 EDX spectra taken close to the edge of the disc. Pb, I and C signals correspond to $MAPbI_3$ while Si and O are signatures of the substrate.

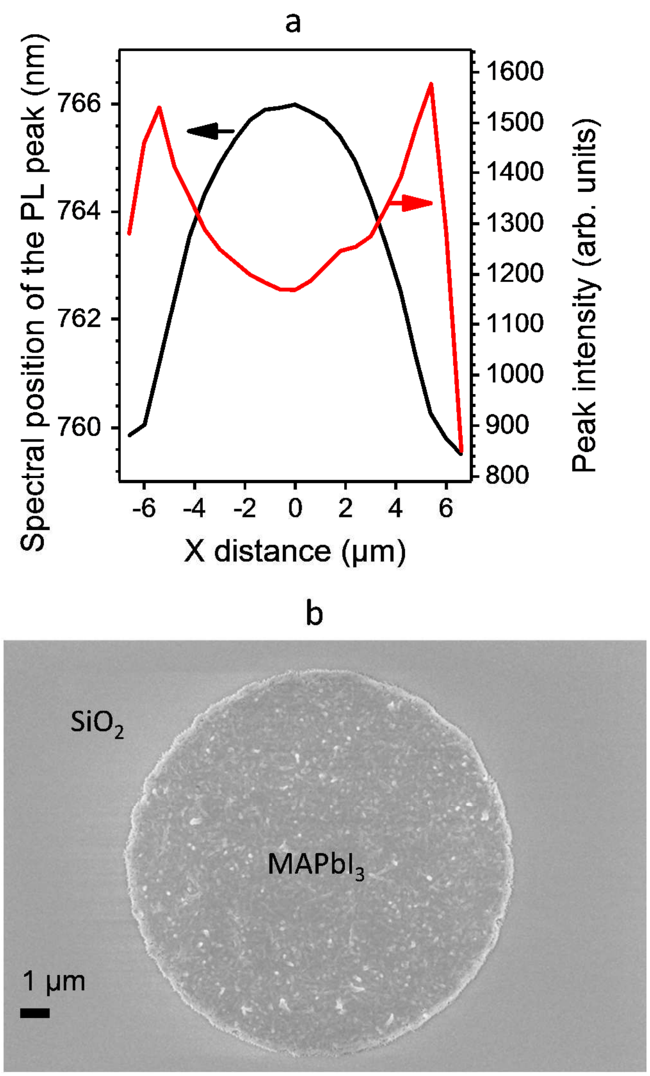

Figure S 7 a) Wavelength of photoluminescence peak vs spatial position (black line) of $MAPbI_3$ disc. Peak emission intensity vs. spatial position (red). The material was excited by 532 nm laser with 50 nW continuous power. b) SEM micrograph of corresponding perovskite disc.

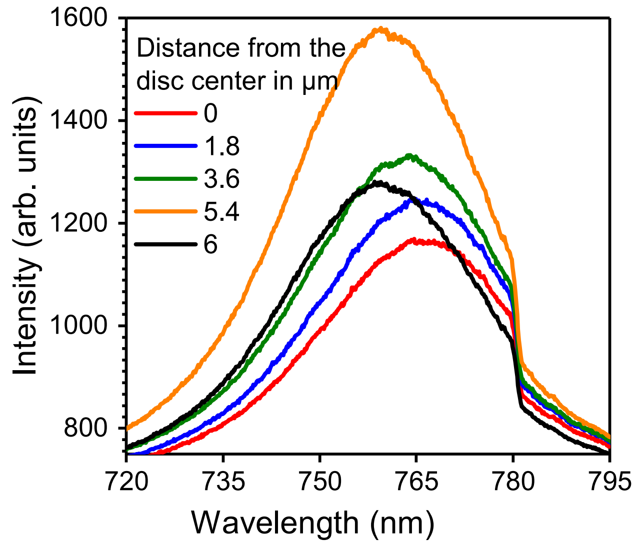

Figure S 8 Spectra collected at points with increasing distance from the disc center.

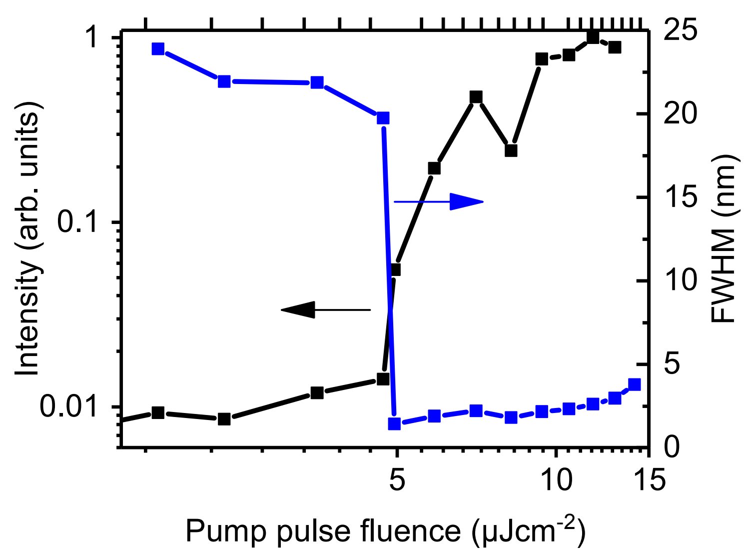

Figure S 9 Full width at half maximum (FWHM) of disc's emission vs. pump power (blue) and emission intensity (black) vs. pump pulse fluence. In the multimode operation regime FWHM and emission intensity of the most intense lasing mode was taken into account.

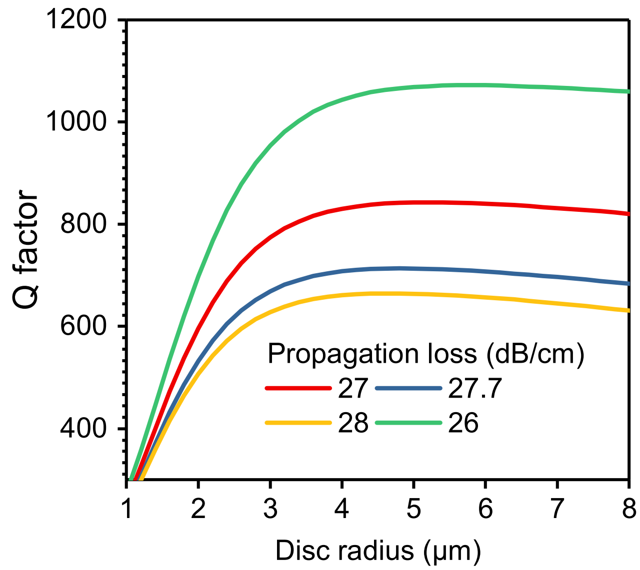

Figure S 10: Q factor dependency on the disc radius for various propagation loss in the perovskite material. Losses of 27.7 dB/cm give the best match with measured quality factors (Q).

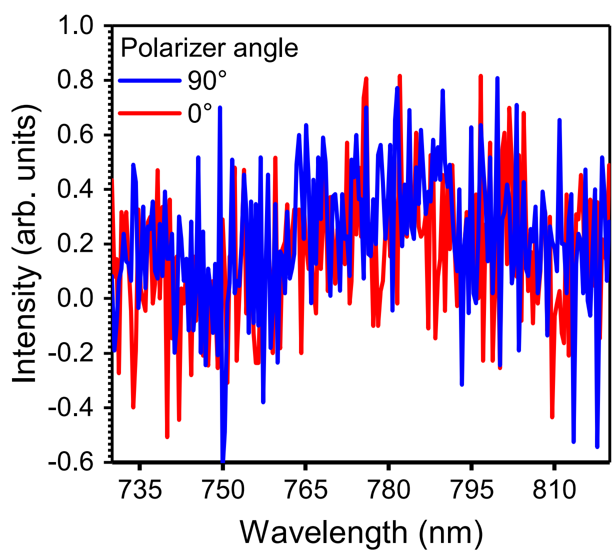

Figure S 11: Signal from the laser below threshold taken at 0 and 90° polarizer angle.

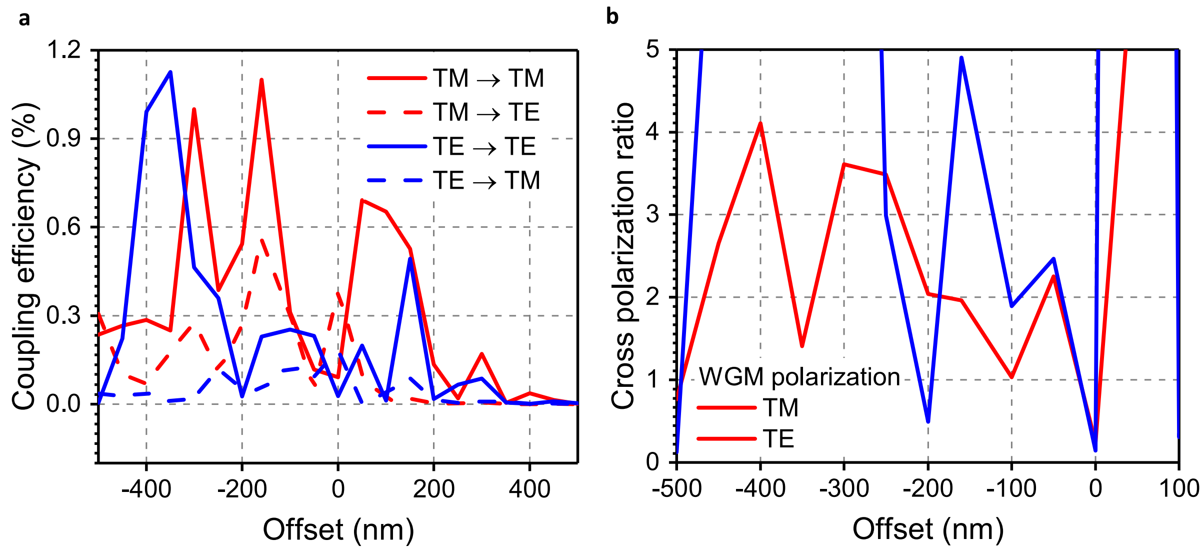

Figure S 12 a) Comparison of coupling efficiency of TM WGM to both TM and TE waveguides modes obtained by the simple and rough models. b) Dependency of ratio of coupling efficiency of TM WGM to TM and TE modes on the bus waveguide offset.

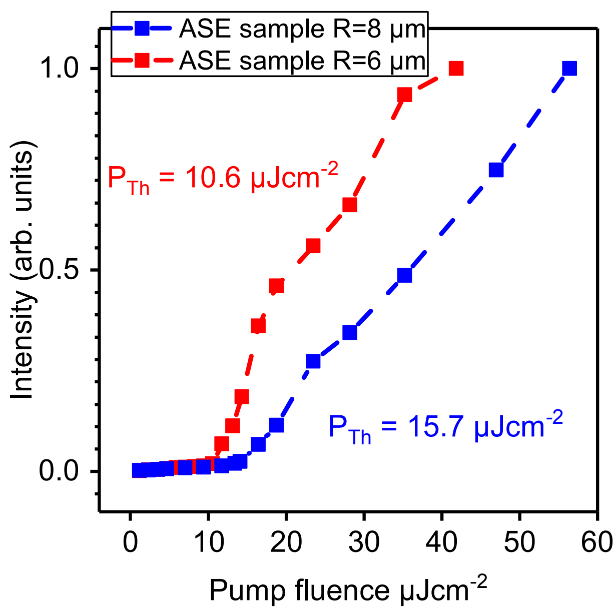

Figure S 13 Output intensity vs. pump fluence of ASE measured using 15 μm wide perovskite waveguides.

V. References:

(1) Quan, H.; Guo, Z. *J. Micro/Nanolithography, MEMS, MOEMS* **2009**, *8*, 033060.

(2) Hammer, M.; Ivanova, O. V. *Opt. Quantum Electron.* **2009**, *41*, 267–283.